Available online at www.sciencedirect.com
ScienceDirect
Ceramics International 34 (2008) 1857–1865
CERAMICS INTERNATIONAL
www.elsevier.com/locate/ceramint

Study of the resistance to crack propagation in alumina by acoustic emission

S. Bouras *, I. Zerizer, F. Gheldane, M.T. Bouazza, B. Bouzabata

Laboratoire des Matériaux Avancés, Université de Annaba, B.P. 12, 23000 Annaba, Algeria

Received 7 March 2006; received in revised form 4 February 2007; accepted 29 June 2007
Available online 19 August 2007

Abstract

The resistance to crack propagation or R-curve effect is still extensively studied in polycrystalline ceramic materials. This effect is shown in the literature by the increase of the stress intensity factor K_I versus crack extension, or by the decrease of crack velocity versus K_I under flexure tests. We have studied this fracture resistance by using the acoustic emission and the Hertzian indentation technique. It was found that the acoustic emission count rate decreases, like crack velocity in conditions of sub-critical crack growth before the failure is reached. Two specimen of alumina, respectively with small and coarse grains, were tested. A high crack extension resistance is obtained for coarse-grained alumina. Mechanisms of crack bridging and crack shielding are responsible for the R-curve effect. These mechanisms are also operating during cyclic loading. The resistance to crack propagation increases more and more after each cycle. Also we obtain R-curve effect during static loading.

On the other hand, toluene or silicone oil corrosive environment delays the crack propagation. But water medium has a reverse effect and the apparent toughness is reduced in this case.

Keywords: Hertzian indentation; Acoustic emission; Crack extension; R-curve; Sub-critical growth; Alumina

1. Introduction

1.1. Resistance to crack propagation: R-curve effect

Ceramic brittleness is due to pre-existent micro-cracks which propagate unstably until the failure occurs. Some technical ceramics exhibit a crack growth resistance that leads to stable crack propagation. In this case, the material toughness is no longer constant but increases with the crack extension.

The increase of fracture resistance with crack extension under stable crack growth is due to energy-consuming effects such as micro-cracking [1], crack ramification, bridging by grains [2], crack shielding by a damaged zone, plastic deformation, or phase transformation. This phenomenon is called R-curve behavior and is associated with the stress intensity factor K_I: additional energy is necessary for a crack to propagate until failure occurs, because of residual compressive stresses appearing in the crack wake and tending to close it. The roughness of the fracture surfaces permits physical contact between them as long as the crack does not open too much.

1.2. Sub-critical crack growth

The sub-critical crack growth is one of the most frequent propagation modes in ceramics. It occurs under stress lower than the critical stress for fracture. Slow crack growth is most suitably described by a relation between the crack velocity V and the stress intensity factor K_I in a K_I–V diagram (Fig. 1). In stage I, at low applied stresses, the crack velocity depends closely on K_I. For intermediate stresses or stage II, the propagation continues with constant speed. At high stresses, the velocity becomes again very sensitive to K_I in the stage III. V depends on the chemical environment, on the loading mode [3] and on the initial flaw size [4], but is independent of the specimen geometry.

The catastrophic fracture of a component occurs at the critical value K_{IC}. K_{I0} is a threshold limit [5] below which no crack growth appears. It permits us to define a safety domain for the specimen.

* Corresponding author.

0272-8842/$34.00
doi:10.1016/j.ceramint.2007.06.015

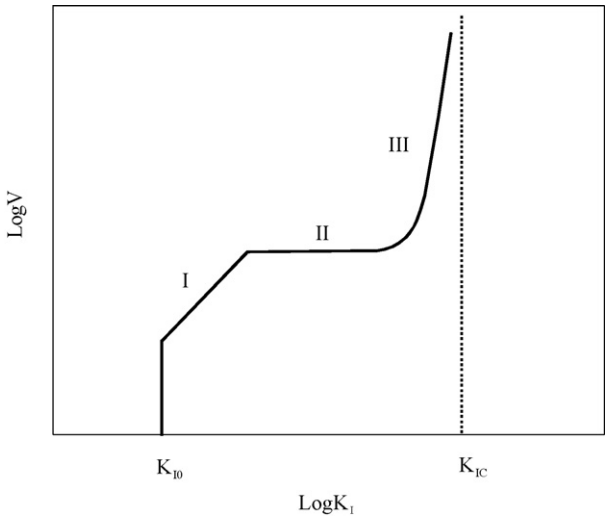

Fig. 1. Crack velocity as a function of applied stress intensity factor (K_I–V diagram).

In the stage I, the growth rate is controlled by a corrosion reaction at the crack tip. The variation of V versus K_I is described by the following law:

$$V = AK_I^n \quad (1)$$

where A and n are constants that characterize the material and its environment respectively.

In the stage II, the growth rate is controlled by the diffusion of corrosive species towards the crack tip [6,7].

In the stage III, governed also by a similar law as relation (1), the driving force is higher and the failure is imminent. This stage is due to different mechanisms: thermally activated growth, growth controlled by a dislocation process, etc. [7,8].

Different sub-critical growth behaviors due to an R-curve effect have been observed in the case of a macro-crack (initiated from a notch in bending) or of natural flaws (pores, inclusions, etc.) [3,9–11]. This R-curve effect, with a decrease in velocity, is well observed at the start of the macro-crack growth and tends towards saturation (Fig. 2). When the driving force becomes closer to K_{IC} and the propagation rate quickly increases, the behavior becomes similar to that of natural cracks.

The R-curve effect in alumina was studied by Fett and Munz [10–12]. The K_I–V curves for macro-cracks show an initial decrease followed by an increase of velocity up to a catastrophic failure. A similar behavior has been observed by Steinbrech [13]. The driving force at the sharp crack tip [14], ''tip stress intensity factor'' K_{tip}, differs from the ''applied stress intensity factor'' K_{appl}, by the stress shielding effect due to the crack surface interaction. In the coarse-grained alumina studied by the authors (grain size is about 20 μm), the shielding process is essentially bridging of the crack surfaces by interlocking grains.

The effective stress intensity factor at the crack tip, K_{tip}, may be written as

$$K_{tip} = K_{appl} - \Delta K_I \quad (2)$$

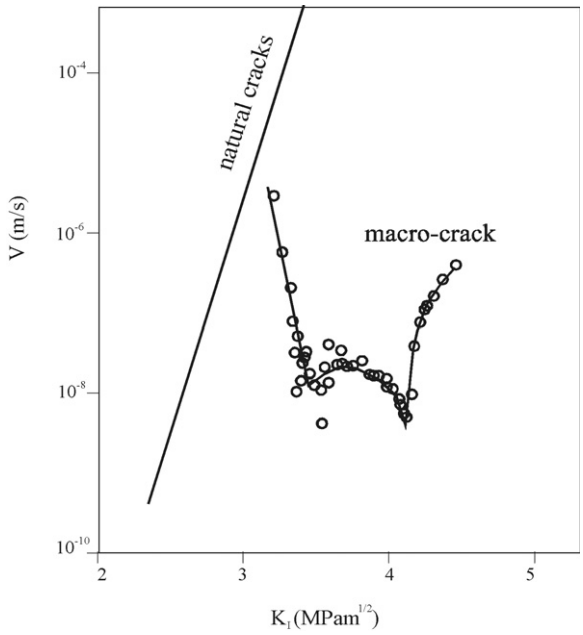

Fig. 2. Sub-critical crack growth under constant load with natural cracks or a macro-crack [9].

where $K_{appl} = \sigma Ya^{1/2}$ is applied by external load and ΔK_I is the contribution of the reinforcement mechanisms. The R-curve effect compensates the effect of the sub-critical growth. This has been shown on alumina and zirconia by Fett and Munz [10,11] using flexure tests under constant load. The authors reported the K_I–V diagram (Fig. 2) that shows a minimum in velocity when K_I increases.

Observations of brittle crystalline solids in the transmission electron microscope by Lawn et al. [14], Hockey and Wiederhorn [15], Hockey and Lawn [16] have revealed inter-facial misfit dislocations which form when crack interfaces rebond in imperfect registry, but no evidence for crack tip plasticity. It is this absence of plasticity which explains why the static fatigue limit of glasses and ceramics corresponds to equilibrium cracks and to the true Griffith criterion.

1.3. Acoustic emission

The acoustic emission (A.E.) designates all manifestation of acoustic waves whose source is within a material undergoing a structural modification induced by an applied mechanical load. When an irreversible energy release occurs, a part is transformed in an emitted stress wave that can be detected with an appropriate sensor.

In the polycrystalline ceramic materials, the sub-critical crack growth, essentially intergranular, is one of the sources of A.E. Because of the microstructure (rigid grain, porosity inclusions, etc.) the crack tip is irregular and the growth occurs by sequential steps along the tip. An A.E. event corresponds at each step. The A.E. method must be highly sensitive and the sensor, even distant from the source, detects the source event. Therefore, it is not necessary to localize the source.

The interest is to acquire data about emissive events and to relate them to their origin mechanisms.

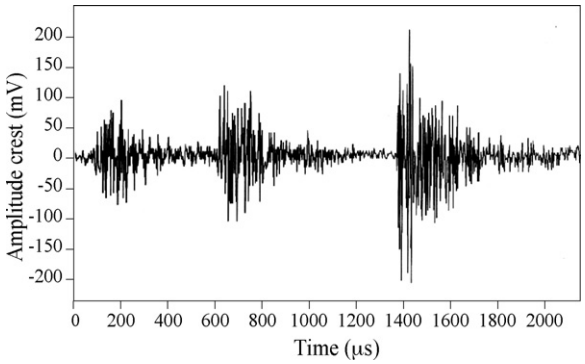

Fig. 3. Burst type signal: amplitude crest to crest.

When the source liberates an energy pulse, the corresponding signal of A.E. is of burst type (Fig. 3). This signal is easily distinguished from the ground noise because of its high amplitude. The signal contains some information concerning the source phenomenon.

Crack propagation is the result of successive jumps of localized parts of the crack front. Each crack jump (an ark) is the source of acoustic emission. A group of arks represents a crack that emits an event (a salvo). Each salvo is represented by an acoustic emission peak in the curves amplitude-time. The events count rate, dN/dt, is a correct image of the average crack growth rate. It is related to the stress intensity factor by a similar equation as relation (1).

Previous works [17,18] have already shown that the events count rate exhibits the same functional dependence on K_1 as does the slow crack velocity. Evans and Linzer [17] showed that the relationship between the events count rate dN/dt and the time-to-failure can be effectively used for the failure prediction. However, this prediction needs a well-characterized material and a well-defined low-level emission. Khuri et al. [19] used acoustic surface wave techniques on polished ceramics for detecting and characterizing surface cracks and also to predict failure. Our experimental conditions of A.E. are close to those used by Evans and Linzer. In fact, the time-to-failure can be measured by A.E.

In the present work, the acoustic emission is detected by a Brüel & Kjær piezoelectric transducer of frequency range 200–300 kHz with a 2–3 μV ground noise. A preamplifier (pass-band filter >200 kHz, gain 40 dB), and an amplifier (variable gain from 0 to 50 dB with a filter of 200 kHz to 2 MHz) are used. After amplification, the signal is memorised in a home made counter. The number of times that it overpasses a given fixed threshold V^* above the noise level (Fig. 4), is recorded as counts N. The counts can be cumulative (cumulative counts: N) or initialized at regular intervals (count rate: dN/dt: number of arks by unit of time).

1.4. Hertzian indentation

In our work, the A.E. technique is used to follow the changes in cracks propagation dynamics in a Hertzian indentation loading. The Hertzian indentation (Fig. 5) is a mechanical characterization method. When a brittle material plane surface

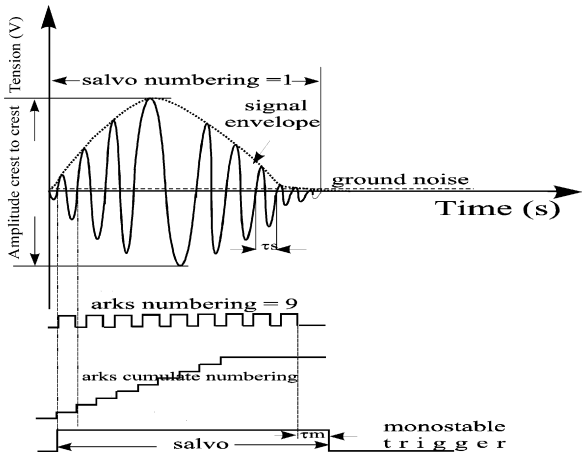

Fig. 4. Numbering of arks of an acoustic emission salvo.

is loaded by a spherical indenter of radius R, a circular crack of radius r_0, forms a minimum critical load $P_C r_0$ is slightly superior to the radius a of the contact zone between the ball and the material. As the load increases, the crack propagates both at the surface over a circle around the contact zone, and in depth as a conical shape crack of length c [20]. ''See Electronic Annex 1 in the online version of this article''. This method needs the presence of natural initial flaws at the surface of the sample. Upon attaining a critical ''Griffith configuration'', a favourably located flaw runs around the contact to form a surface ring crack. The flaws, introduced by polishing, are Griffith elliptic defects with a front curve and become sharp crack after a lifetime [21–24].

Using spheres, flat punches and peeling, Maugis and Barquins [25] and Maugis [26] studied the equilibrium, healing and the propagation of sub-critical Griffith cracks according to the loss of the elasticity at the crack tip in elastic solids, glasses and ceramics. The edge of the contact area can be considered as an interface crack tip in mode I such that the system is the same for a notched solid with an imposed crack path. Maugis has also widely evoked the Griffith criterion at the crack tip local conditions.

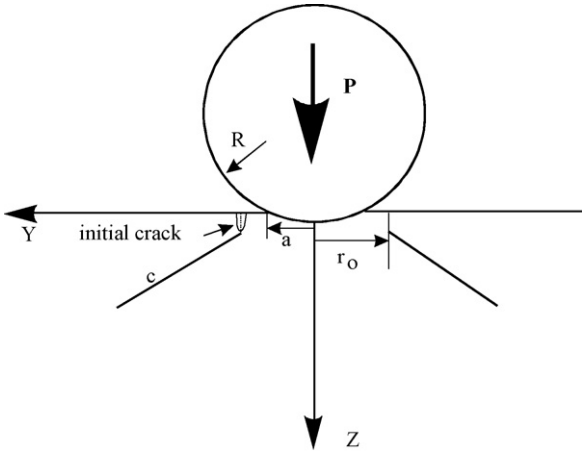

Fig. 5. Schematics of the Hertzian contact: a contact radius; r_0 crack radius at the surface; c crack length in depth; R ball radius; P indentation load.

The mechanism of cone crack initiation and propagation is well understood by using the Hertz–Huber stress tensor and fracture mechanics [24,27–30]. Sneddon [31] has given the stress field.

In brittle materials, the Hertzian crack is catastrophically produced in a very short time. However, in materials exhibing an R-curve effect, the crack occurs progressively as loading proceeds: small cracks are initiated from random flaws to form relatively deep circle arc that coalesce in a circular crack at the surface, and in a conical crack in depth [32].

The critical value P_C corresponding to the final unstable crack extension is determined by the A.E. event of the highest amplitude. The crack jumps occurring before reaching P_C produce acoustic emission events of small amplitudes.

The A.E. monitoring is then a tool for following the resistance to crack propagation step by step. It can also be used to determine the fracture surface energy and the toughness by using classical theories of the Hertzian indentation [29,30,33–41].

Initial flaws of a chosen size are introduced by using a polishing paper of a specific abrasion grit size [21,32]. The balls used in the present work have the following characteristics: cemented carbide 94WC–6Co, density: 15 g/cm^3, hardness: 1550 Hv, E = 630 GPa, $\upsilon = 0.22$, radius from 1 to 14 mm. They have been provided by CIMAP-France.

2. Description of the materials

We studied two alumina ceramics. The first material has been processed by G.E.M.P.P.M (Groupe d'Etudes de Métallurgie Physique et de Physique des Matériaux) laboratory (Fig. 6a) from an alumina powder (99.9% purity). Sintered at 1550 °C under an applied uniaxial load of 40 MPa, the resulting grain size is between 2 and 10 μm. The second material (Fig. 6b), an industrial alumina provided by Desmarquet Céramiques et Techniques (code AF997, 99.8% purity), has been sintered at 1600 °C ending in coarse grains with sizes between 5 and 20 μm.

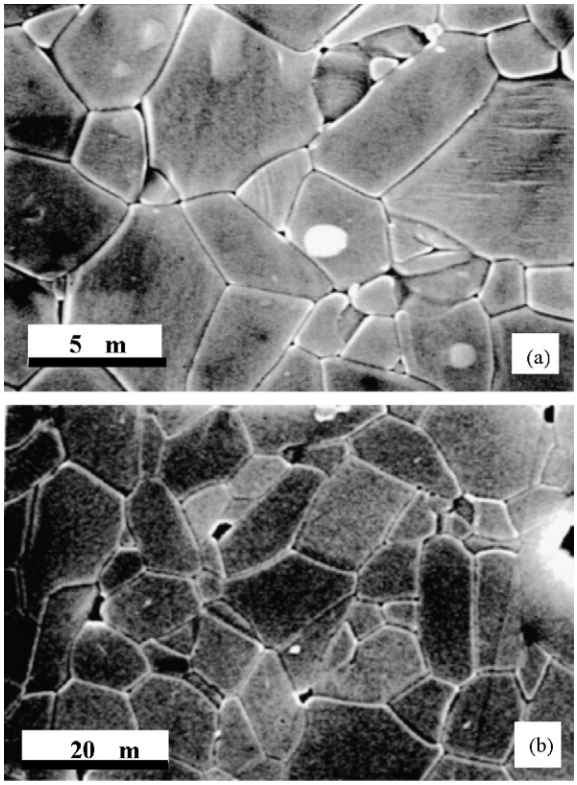

Fig. 6. Microstructure of alumina: (a) elaborated in laboratory (small grains) and (b) industrial alumina (coarse grains).

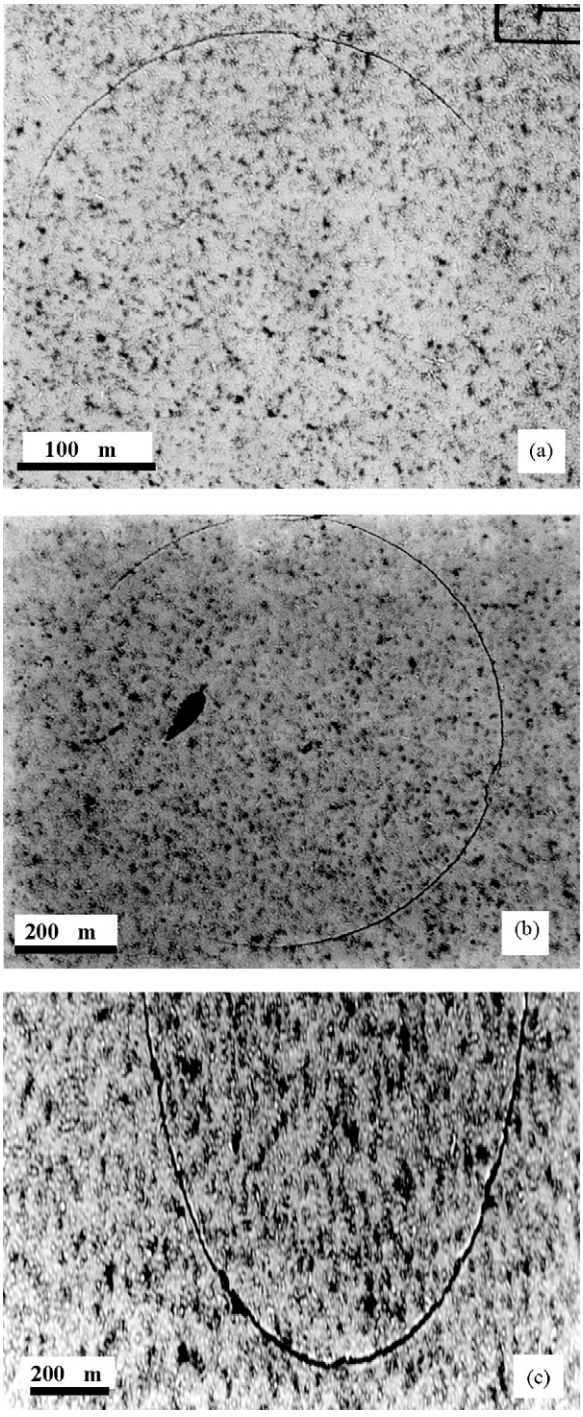

Fig. 7. Stages of a circular fissure formation. Laboratory alumina (small grains); grit size 3 μm: (a) P_{max} = 700 N, R = 4 mm; (b) P_{max} = 950 N, R = 8 mm; (c) P_{max} = 1350 N, R = 3 mm.

3. Results

Under Hertzian indentation loading, the circular and conical cracks do not occur immediately. They are formed gradually by progression and propagation of the initial crack (Fig. 7) until the formation of a complete circle whichever the used loading mode (monotonous, static, or cyclic). This effect is due to an increase of the crack propagation resistance (R-curve effect).

Fig. 7 shows the various steps of formation of a circular fissure resulting from loading up to the loads of 700 N (Fig. 7a), 950 N (Fig. 7b), and 1350 N (Fig. 7c) followed by an unloading. The AE activity for the load of 1450 N higher than P_C is given in Fig. 8. The crest amplitude value of the highest A.E. peak corresponding to the critical load P_C, given by the relation $dB = 20 \log_{10} V + 60$ [32], where V is the recorded voltage, is 57 dB. This event peak recorded at 580 s corresponds to the closing of the partial circle as observed (Fig. 7c).

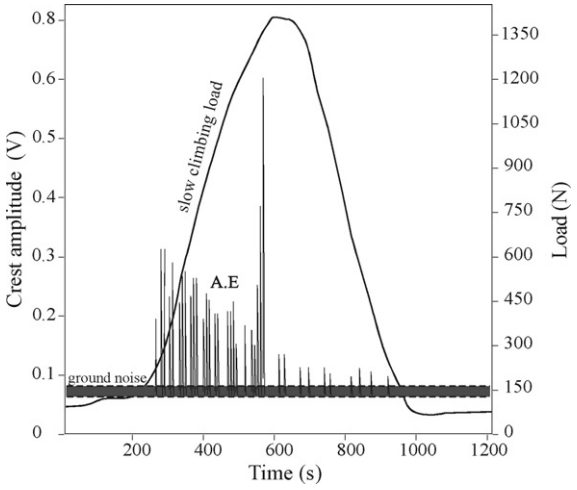

Fig. 8. Acoustic emission during loading up to a load P_{max} (1450 N) higher than P_C. Laboratory alumina (small grains); grit size 3 μm; $R = 4$ mm.

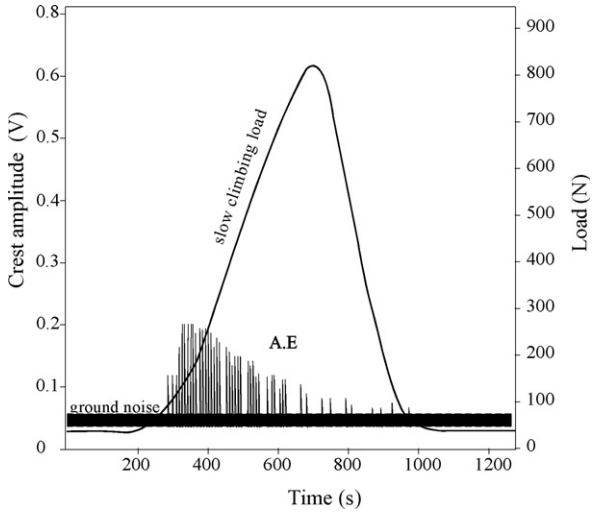

Fig. 9. Acoustic emission for loading up to a load of 820 N lower than P_C. Laboratory alumina (small grains); grit size 3 μm; $R = 3$ mm.

The acoustic activity recorded before reaching P_C (Fig. 9) is similar to the A.E. activity shown on the left of the higher event observed in Fig. 8. These acoustic signals obtained during loading below the critical load are linked to sub-critical crack propagation. In fact, this A.E. activity has already been shown by Nadeau [42] as caused by the interaction between the moving crack and defects on surface.

When a crack is initiated at a favourable flaw, it propagates along a certain proportion of the length of a circle of radius r_0 (partial circular crack), at the surface. Its radius does not change with the increase of the load. And by further loading, the partial circular crack will grow by following the same path of radius r_0, in conformity with the Hertzian stress field.

The number N of A.E. events increases under the effect of the increasing applied load, first slowly, then quickly as the unstable propagation and the failure become imminent (Fig. 10). And below P_C, the events count rate decreases because of small A.E. activity (Fig. 11) revealing an increase of the R-curve effect. This change in events count rate is qualitatively similar to the variation of crack velocity if one assumes that each A.E. event corresponds to a step of a crack

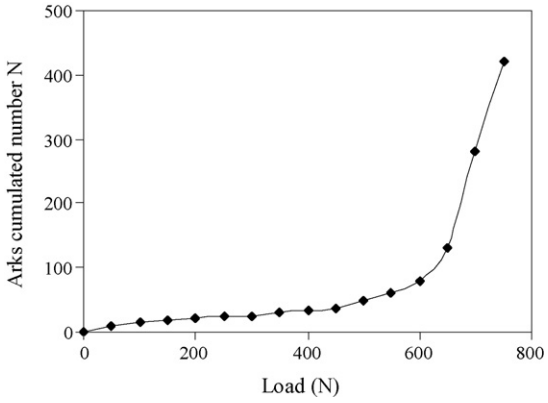

Fig. 10. Typical A.E. events count as a function of load ($P_{max} = 750$ N). Laboratory alumina (small grains); grit size 3 μm; $R = 3$ mm.

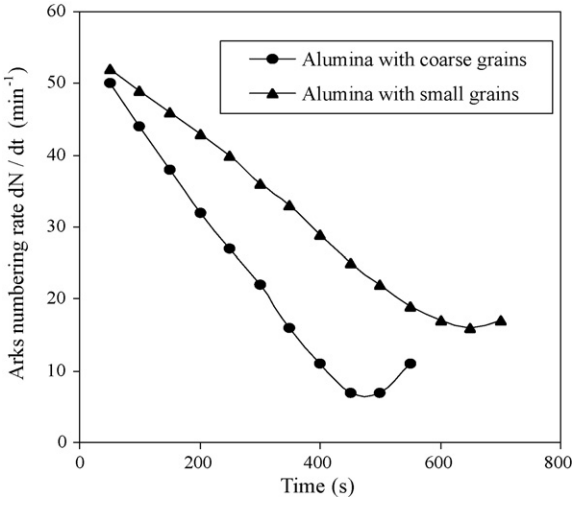

Fig. 11. Events count rate until a load below the critical load P_C ($P_{max} = 750$ N).

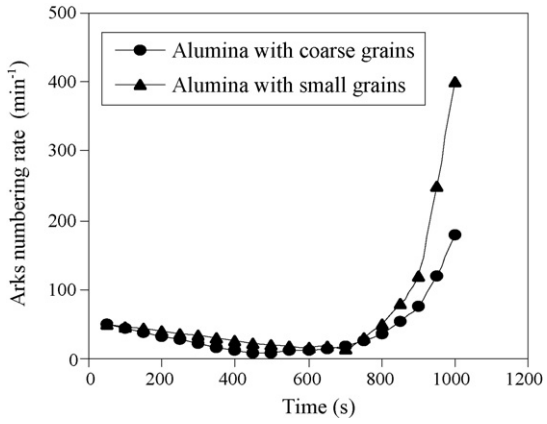

Fig. 12. Events count rate until a load close to the critical load P_C (P_{max} = 1000 N).

increment. Besides, the amplitude of the A.E. peaks decreases (Figs. 8 and 9) indicating that the crack increment steps become smaller. Above P_C, as the load becomes closer to the unstable propagation condition, a very fast rise in count rate is observed (Fig. 12) with peaks of higher amplitudes.

As observed in Fig. 11, the resistance to crack propagation is higher in coarse-grained alumina. This figure points out also that the starting of fracture occurs earlier for coarse-grained alumina. But, because of the R-curve effect, the final fracture will occur later than in the case of fine-grained alumina as Fig. 12 shows. However, the R-curve effect in coarse-grained alumina is often depending on the material microstructure type and on testing conditions [43–46]. Bradt and Scott [43] showed also that the effect of the reinforcement is important as the grain size increases. But, for a lower grain size of 2 or 3 μm, the R-curve is flat and independent of the crack length.

We have also studied the R-curve effect under a constant applied load at about $P \sim 0.80\ P_C$ (reached with a very fast loading) as it is shown in Fig. 13. As depicted, the events count rate, as well as the amplitude of the signals, decrease from the resistance to crack propagation.

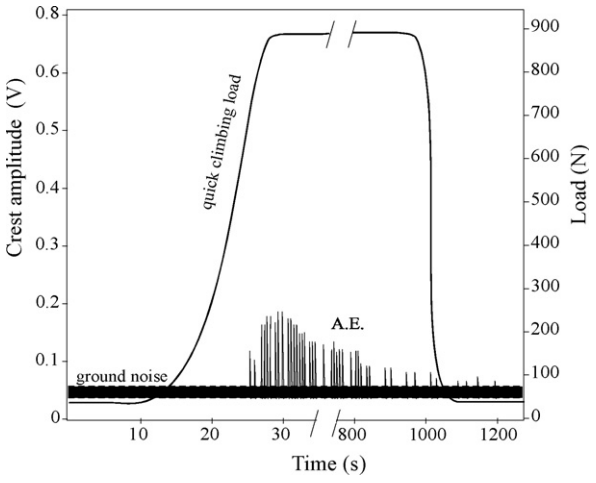

Fig. 13. A.E. activity under constant load as a function of time. Laboratory alumina (small grains); grit size 3 μm; R = 3 mm.

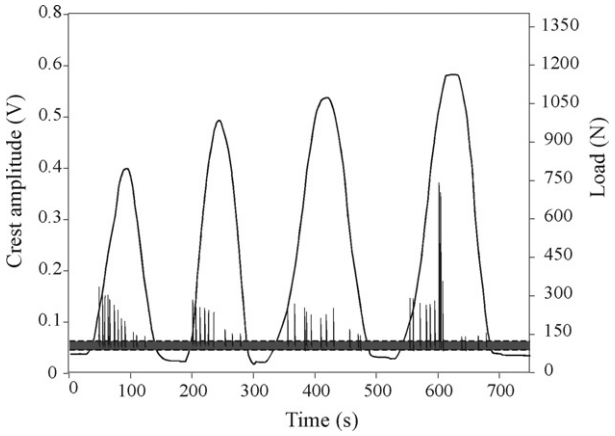

Fig. 14. A.E. Activity under cyclic loading. Laboratory alumina (small grains); grit size: 3 μm; R = 3 mm.

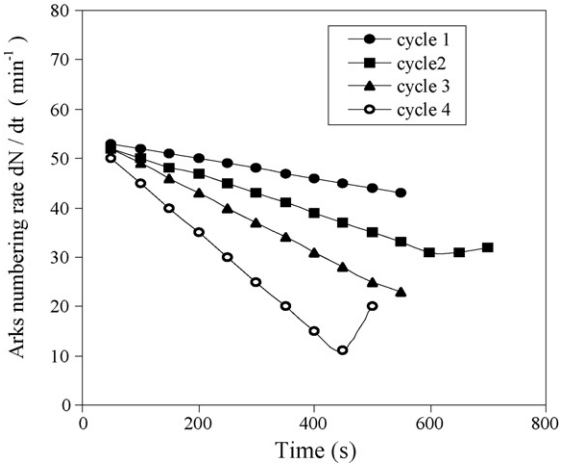

Fig. 15. Detail of events count rate during each of the cycles shown in Fig. 14.

We also carried out successive cycles of loading–unloading (Fig. 14). After every cycle, the structure presents damaged zones (crack shielding) that are taken in consideration by the following cycle. The last cycle continues until the failure of the sample occurs. Before this critical event, the count rate decreases rapidly during each cycle as Fig. 15 shows, indicating again an increase in crack growth resistance associated with more efficient crack shielding. At the approach of the fracture (cycle 4), the events count rate increases: the crack reaches a critical length provoking the failure.

The resistance to crack propagation was also studied by changing the medium (water, toluene, silicone oil). The environment modifies the crack behavior and shows clearly a difference in apparent resistance to crack propagation therefore in apparent toughness. The tests are carried out at P_C. As it is seen in Fig. 16, the presence of the toluene or the silicone oil delays the unstable event and requires a higher critical load than the one required in air. The presence of water has an inverse role and provokes the critical event earlier. During loading under aggressive medium like water, the size of the initial flaw increases by sub-critical crack growth and becomes unstable with a lower P_C value. So, the apparent toughness is reduced in that case.

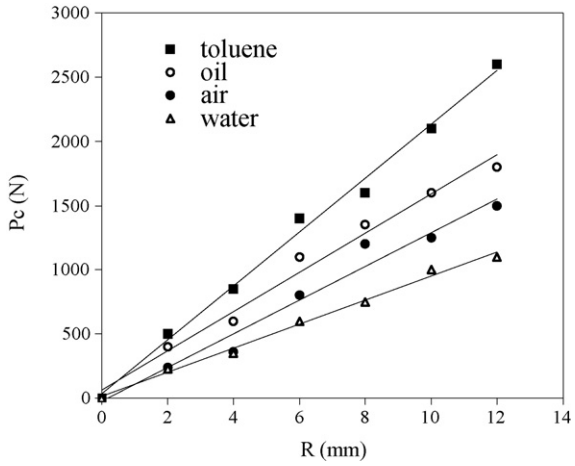

Fig. 16. Hertzian critical load as a function of ball radius for different environments. Laboratory alumina (small grains); grit size 3 μm.

The effect of slow crack growth, below P_C, is depicted in Fig. 17. It shows schematically, in different mediums, the driving force G as a function of the initial flaw size c for different applied loads. In the absence of sub-critical crack growth, the initial flaw size is c_i and the critical load for an unstable jump is P_{Ci}. The unstable jump occurs when the driving force equals the crack growth resistance ($G = 2\gamma f = G_C$). After this jump, the growth becomes stable, needing an increase of loading for failure. In the case of sub-critical crack growth with water environment, the same flaw of size c_i begins to grow in a sub-critical manner under the driving force G_4 ($<G_C$) corresponding to the load P_{C4} ($<P_{Ci}$). So the flaw will grow from c_i up to the size c_4 where it becomes unstable. Water is more corrosive and the critical driving force is consequently weaker than in the other environment cases as in air, silicone oil and toluene. This diagram also shows the influence of the initial flaw size. Smaller c_i implies higher critical loads P_C as it is seen in Fig. 18.

Table 1 shows the critical crack growth energy γf (or G_C) and the apparent fracture toughness K_{IC} values calculated from

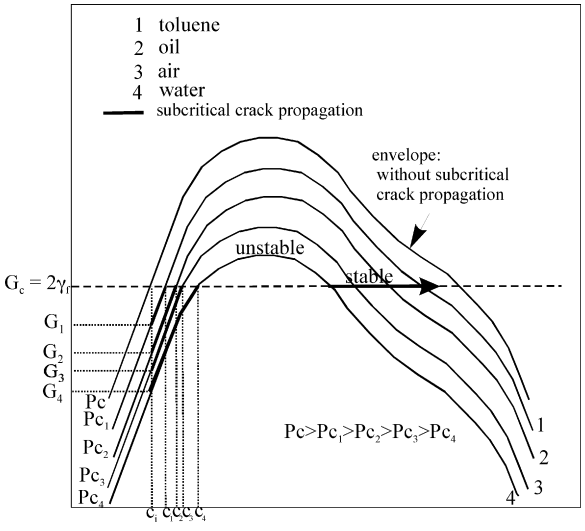

Fig. 17. Schematics of the driving force vs. the crack length.

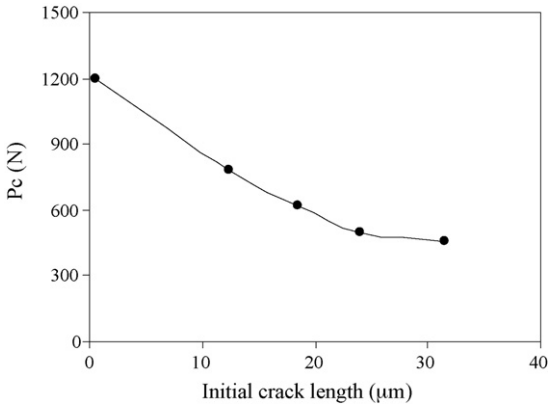

Fig. 18. Variation of the critical load P_C as a function of initial flaw size.

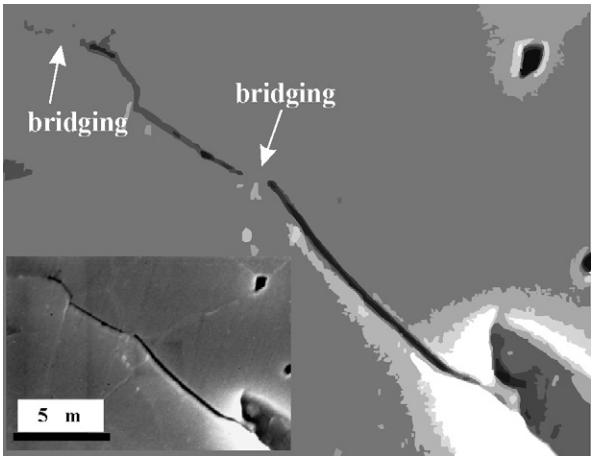

Fig. 19. Vectorisation of the original photo (at the bottom on the left) showing crack bridging sites. industrial alumina 3 μm; $R = 4$ mm; $P_{max} = 1600$ N.

the Hertzian indentation theory. All γf values are higher for coarse-grained alumina. This grain size effect suggests a crack shielding mechanism involving the bridging of the crack surfaces by sliding grains.

The surface crack observations suggest that the R-curve effect is due to crack bridging by grains (Fig. 19) and to the crack shielding by damaged zones (Fig. 20). In any case, the Hertzian indentation provokes a lot of damages, due to the

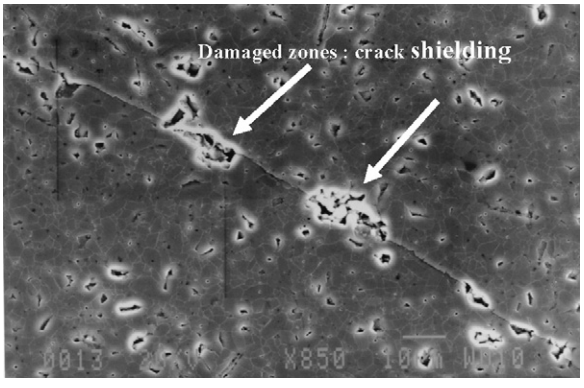

Fig. 20. Photo of microstructure showing damaged zones. Laboratory alumina 3 μm; $R = 3$ mm; $P_{max} = 1800$ N.

Table 1
Results of fracture surface energy (γf) and apparent toughness (K_{IC})

Environment	γf (J m^{-2})		K_{IC} apparent (MPa m$^{1/2}$)	
	Coarse grain alumina	Small grain alumina	Coarse grain alumina	Small grain alumina
Toluene	49.3	43.1	6.2	5.8
Silicone oil	40.2	33.4	5.6	5.1
Air	32.1	27.1	5.0	4.6
Water	24.8	20.5	4.4	4.0

contact with the ball. Most of these damaged zones are the cause of crack slackening.

Comparatively to flexure tests (three-points bending) [45–47] where, at the beginning of the crack propagation, the bridging interactions between the crack surfaces occur in a zone that spreads over the whole of crack length. When this zone increases, the driving force at the crack tip decreases and consequently an apparent crack growth resistance appears. So, for a given crack increment, the bridging zone becomes stationary and translates in the wake of the advancing crack tip. Then the crack growth resistance becomes constant.

4. Conclusions

The resistance to crack propagation under Hertzian indentation was studied on coarse and fine-grained alumina. With the help of acoustic emission, this mechanical characterization method permits easy detection of the R-curve effect. The decrease of the events count rate prior to failure, illustrates the presence of a sub-critical crack growth mechanism. This effect is observed under monotonous, static or cyclic loadings. It is also found that a coarser grain has high resistance crack propagation.

Environments influence crack propagation by stress corrosion at the crack tip. Calculated apparent toughness for four environments leads to classify them regarding the increasing corrosion effect as: toluene, silicone oil, air and water.

The R-curve effect results are in agreement with those obtained by flexure tests.

Acknowledgments

The authors thank the ceramics group (GEMPPM-INSA, Lyons) for their help.

Appendix A. Supplementary data

Supplementary data associated with this article can be found, in the online version, at doi:10.1016/j.ceramint.2007.06.015.

References

[1] A.G. Evans, K.T. Faber, Crack growth resistance of microcracking brittle materials, J. Am. Ceram. Soc. 67 (4) (1984) 255–260.
[2] M.V. Swain, R-curve behavior in a polycrystalline alumina material, J. Mater. Sci. Lett. 5 (4) (1986) 1313–1315.
[3] B.J. Pletka, S.M. Wiederhorn, A comparison of failure predictions by strength and fracture mechanics techniques, J. Mater. Sci. 17 (1982) 1247–1268.
[4] A. Okada, N. Hirosaki, Subcritical crack growth in sintered silicon nitride exhibiting a rising R-curve, J. Am. Ceram. Soc. 73 (7) (1990) 2095–2096.
[5] B.R. Lawn, Fracture of Brittle Solids, Cambridge University Press, 1993.
[6] R.J. Charles, Dissolution behavior of macroporous glass, J. Am. Ceram. Soc. 47 (1964) 154–155.
[7] J.R.J.B. Wachtman, Highlights of progress in the science of fracture of ceramics and glass, J. Am. Ceram. Soc. 57 (12) (1974) 509–519.
[8] F.F. Lange, In Deformation of Ceramic Materials, Pensylvania State University, Plenum Press, 1975, pp. 361–381.
[9] T. Fett, D. Munz, Evaluation of subcritical crack extension under constant loading, J. Eur. Ceram. Soc. 6 (1990) 67–72.
[10] T. Fett, D. Munz, Subcritical crack growth of macrocracks in alumina with R-curve behavior, J. Am. Ceram. Soc. 75 (4) (1992) 958–963.
[11] T. Fett, D. Munz, Subcritical crack growth of macrocracks in zirconia, J. Mater. Sci. Lett. 10 (1991) 1103–1106.
[12] T. Fett, D. Munz, Subcritical crack growth of macro- and microcracks in ceramics, in: R.C. Bradt, et al. (Eds.), Fracture Mechanics of Ceramics, 9, Plenum Press, New York, 1992, p. 604.
[13] R.W. Steinbrech, R-curve behavior of ceramics, in: R.C. Bradt, et al. (Eds.), Fracture Mechanics of Ceramics, 9, Plenum Press, New York, 1992, pp. 187–208.
[14] B.R. Lawn, B.J. Hockey, S.M. Wiederhorn, Atomically sharp cracks in brittle solids: an electron microscopy study, J. Mater. Sci. 15 (5) (1980) 1207–1223.
[15] B.J. Hockey, S.M. Wiederhorn, Crack healing in brittle materials, in: R.C. Bradt, et al. (Eds.), Fracture Mechanics of Ceramics, 6, Plenum Press, New York, 1983, p. 637.
[16] B.J. Hockey, B.R. Lawn, Electron microscopy of microcracking about indentationsin aluminum oxide and silicon carbide, J. Mater. Sci. 10 (8) (1975) 1275–1284.
[17] A.G. Evans, M. Linzer, Failure prediction in structural ceramics using acoustic emission, J. Am. Ceram. Soc. 56 (11) (1973) 575–581.
[18] A.G. Evans, M. Linzer, L.R. Russel, Acoustic emission and crack propagation in polycrystalline alumina, Mater. Sci. Eng. 15 (1974) 253–261.
[19] B.T. Khuri-Yakub, A.G. Evans, G.S. Kino, Acoustic surface wave measurements of surface cracks in ceramics, J. Am. Ceram. Soc. 63 (1/2) (1980) 65–71.
[20] S. Bouras, D. Rouby, G. Fantozzi, Application de la Technique de l'Emission Acoustique dans l'Etude de l'Indentation Hertzienne, Revue des Composites et des Matériaux Avancés 5 (2) (1995) 235–252.
[21] F.B. Langitan, B.R. Lawn, Hertzian fracture experiments on abraded glass surfaces as definitive evidence for an energy balance explanation of Auerbach's Law, J. Appl. Phys. 40 (10) (1969) 4009–4017.
[22] B.R. Lawn, D.B. Marshall, Indentation fracture and strength degradation in ceramics, in: Proceedings of the International Symposium on Fracture Mechanics of Ceramics, University Park, PA, USA, July 27–29, 1977, (1978), pp. 205–229.
[23] T.R. Wilshaw, The Hertzian fracture test, J. Phys. D.: Appl. Phys. 4 (1971) 1567–1581.
[24] B.R. Lawn, Partial cone crack formation in a brittle material loaded with a sliding spherical indenter, Proc. R. Soc. A299 (1967) 307–316.
[25] D. Maugis, M. Barquins, Fracture mechanics and the adherence of viscoelastic bodies, J. Phys. D.: Appl. Phys. 11 (1978) 1989–2023.

[26] D. Maugis, Review subcritical crack growth, surface energy, fracture toughness, stick-slip and embrittlement, J. Mater. Sci. 20 (1985) 3041–3073.
[27] M.T. Huber, On the theorie of contacting solid elastic bodies, Ann. Phys. 14 (1904) 153–163.
[28] A.E.H. Love, The stress produced in a semi-infinite solid by pressure on part of the boundary, Philos. Trans. R. Soc. Lond. A 228 (1929) 377–420.
[29] R. Mouginot, D. Maugis, Fracture indentation beneath flat and spherical punches, J. Mater. Sci. 20 (1985) 4354–4376.
[30] R. Warren, Measurements of the fracture properties of brittle solids by Hertzian indentation, Acta Met. 26 (1978) 1759–1769.
[31] N. Sneddon, Boussinesq's problem for a flat-ended cylinder, Proc. Camb. Philos. Soc. 42 (1946) 29–39.
[32] S. Bouras, Etude par Emission de l'Indentation Hertzienne et de l'Indentation Vickers sur une Vitro-céramique et sur des Alumines, Thèse de Doctorat d'Etat, INSA de Lyon (1993) 186.
[33] F.C. Frank, B.R. Lawn, On the theorie of Hertzian fracture, Proc. R. Soc. A299 (1967) 291–306.
[34] B.R. Lawn, Indentation of ceramics wit, spheres: a century after Hertz, J. Am. Ceram. Soc. 81 (1998) 1977–1994.
[35] B.R. Lawn, T.R. Wilshaw, Review-indentation fracture: principles and applications, J. Mater. Sci. 10 (6) (1975) 1049–1081.
[36] H. Hertz, On the contact of elastic solids, Zeitschrift für die Reine und Angewandte Mathematik 92 (1881) 156–171, English translation in Miscellaneous Papers (translated by D.E. Jones, G.A. Schott), Macmillan, London, U.K. (1896) pp. 146–162.
[37] H. Hertz, On the contact of rigide elastic solids and on hardness, Verhandlungen des Vereins zur Beförderung des Gewerbefleisses 61 (1882) 449–462, English translation in Miscellaneous Papers (translated by D.E. Jones, G.A. Schott), Macmillan, London, U.K. (1896) pp. 163–183.
[38] F. Auerbach, Absolute hardness measurements, Ann. Phys. Chem. 43 (1891) 61–100.
[39] F.C. Roesler, Brittle fractures near equilibrium, Proc. Phys. Soc. B69 (1956) 981–992.
[40] P.D. Warren, D.A. Hills, The influence of elastic mismatch between indenter and substrate on Hertzian fracture, J. Mater. Sci. 29 (1994) 2860–2866.
[41] J.P.A. Tillet, Fracture of glass by spherical indenters proc, Phys. Soc. B69 (1956) 47–54.
[42] J.S. Nadeau, Acoustic emission in the fracture of glass plates, J. Am. Ceram. Soc. 64 (10) (1981) 585–590.
[43] R.C. Bradt, W.D. Scott, Mechanical properties of alumina, in: L.D. Hart (Ed.), Alumina Chemicals Science and Technologie Handbook, The American Ceramic Society, Columbus, Ohio, 1990, pp. 23–39.
[44] M.E. Ebrahimi, J. Chevalier, M. Saadaoui, G. Fantozzi, Effect of grain size on crack growth in alumina, in: R.C. Bradt, et al. (Eds.), Fracture Mechanics of Ceramics, 13, Kluwer Academic/Plenum Publishers, 2002 pp. 273–286.
[45] M. Saadaoui, Contribution à l'étude du comportement thermomecanique des matériaux céramiques à effet de courbe-R: choc et fatigue thermiques, Thèse de Doctorat d'Etat, INSA de Lyon (1996) 175.
[46] D. Bleise, R.W. Steinbrech, Flat R-curve from stable indentation cracks in coarse-grained alumina, J. Am. Ceram. Soc. 77 (2) (1994) 315–322.
[47] G. Fantozzi, J. Chevalier, M. Saadaoui, R-curve effect on slow crack growth and thermal shock of ceramics, in: R.C. Bradt, et al. (Eds.), Fracture Mechanics of Ceramics, 13, Kluwer Academic/Plenum Publishers, 2002, pp. 213–228.